Performance of hydroxyapatite-supported catalysts for methane production via CO_2 hydrogenation on semi-pilot scale

de Medeiros, Fábio Gonçalves Macêdo; Farzi, Farbod; Achouri, Ines Esma; Lotfi, Samira; Rego de Vasconcelos, Bruna

Publisher's version / Version de l'éditeur:
https://doi.org/10.1007/s12649-023-02106-7
Waste and Biomass Valorization, 2023-03-15

Waste and Biomass Valorization
https://doi.org/10.1007/s12649-023-02106-7

ORIGINAL PAPER

Performance of Hydroxyapatite-Supported Catalysts for Methane Production Via CO_2 Hydrogenation on Semi-Pilot Scale

Fábio Gonçalves Macêdo de Medeiros[1] · Farbod Farzi[2] · Ines Esma Achouri[2] · Samira Lotfi[3] · Bruna Rego de Vasconcelos[1]

Received: 15 July 2022 / Accepted: 27 February 2023

Abstract

Low-carbon methane (CH_4) obtained from CO_2 hydrogenation is a promising option for reducing greenhouse gases (GHG) emissions from carbon-intensive fossil fuel-based energy production, but catalytic performance, especially in low temperatures, still needs to be improved before large-scale implementation. In this work, it is proposed the use of hydroxyapatite (HAP) as an alternative catalyst support to validate its performance for CO_2 hydrogenation to CH_4. In addition, for the first time in literature, the influence of process conditions (temperature, gas hourly space velocity and Ni metal load) on the performance of HAP-supported catalysts is investigated on semi-pilot scale. CO_2 conversion is favored up to 400 °C, despite the thermodynamic limitations of the hydrogenation reaction. Ni-based catalysts present the best performance for CO_2 hydrogenation with a maximum CO_2 conversion around 88% under optimized conditions (20 wt.% Ni, T = 350 °C, GHSV = 320 h^{-1}) with 100% CH_4 selectivity and no CO production up to 450 °C. Finally, long-term operation of 20Ni/HAP for 50 h on semi-pilot scale shows a robust performance with 83% CO_2 conversion, 100% CH_4 selectivity and no signs of catalyst deactivation. The performance HAP-based catalyst presented here demonstrates the feasibility of HAP as alternative catalyst support for CO_2 hydrogenation and the potential for process upscaling with HAP-supported catalysts.

Graphical Abstract

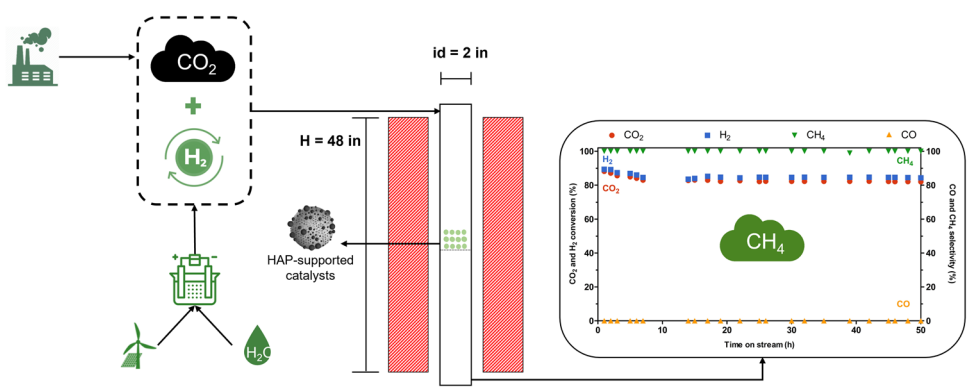

Keywords Hydroxyapatite · CO_2 hydrogenation · Nickel catalysts · Methane · Low-carbon energy vectors

Statement of Novelty

The development of efficient catalysts for CH_4 production from CO_2 hydrogenation is of great interest due to the key aspect of this process for the energy transition. HAP meets the criteria for potential catalyst support, especially related

✉ Bruna Rego de Vasconcelos
bruna.rego.de.vasconcelos@usherbrooke.ca

Extended author information available on the last page of the article

Published online: 15 March 2023

to its tunable surface basicity and thermal stability. However, to the best of our knowledge, only one report in literature has considered its use for CO_2 hydrogenation to CH_4. In the present work, we investigate the influence of process conditions for CO_2 hydrogenation over HAP-supported catalysts on semi-pilot scale and demonstrate the feasibility of the process with a great catalytic performance of Ni-based HAP-supported catalyst. The evaluation of important process parameters on semi-pilot scale provides important and novel information for the potential upscaling of CO_2 hydrogenation process using HAP-supported catalysts.

Introduction

The energy transition towards a low-carbon energy economy is one of the major global challenges and dealing with the greenhouse gas (GHG) emissions has become crucial to achieve this transition [1]. Carbon dioxide (CO_2) accounts for more than 60% of the worldwide GHG emissions and it is a primary contributor for the severe global warming and climate changes [2]. In the efforts for fighting climate changes, countries have turned their attention towards the implementation of policies that limit and reduce CO_2 emissions. The European Union, for example, committed to reducing GHG emissions by 55% below 1990 levels by 2030 [3]. In the Canadian scenario, the government has committed to an emission reduction target of 40–45% below 2005 levels by 2030 [4]. As carbon-intensive energy production from fossil fuels still accounts for more than 80% of the global energy demand [5], the development of processes towards CO_2 emissions reductions and low-carbon energy production are of great practical interest [6].

Carbon capture and utilization (CCU) technologies have been identified as a promising pathway towards a sustainable emissions reduction and the production of low-carbon energy vectors to enable the energy transition [2, 6]. Among the processes considered in the scope of CCU, CO_2 hydrogenation is especially interesting for its flexible operation conditions depending on the wide range of products that can be obtained from such process, such as methane, methanol, higher alcohols, olefins, etc. [7–12]. In this context, CO_2 hydrogenation occurs in two steps: first, low-carbon hydrogen (H_2) is obtained from water electrolysis using renewable electricity. Then, it is combined with CO_2 captured from different processes, including high-emitting industries such as cement, steel and aluminum production, to produce different low-carbon energy vectors [13, 14]. When water electrolysis is used for H_2 production, the production of low-carbon energy vectors via CO_2 hydrogenation is usually referred to as Power-to-X (with the X depending on the end product) [15, 16]. Among the low-carbon energy vectors obtained from CO_2 hydrogenation, methane (CH_4) is of particular interest for accounting for around 23% and 36% of the global and Canadian energy demands, respectively, in 2019 [5, 17], and for being compatible with the current infrastructure for natural gas distribution and utilization [18, 19].

CH_4 production via CO_2 hydrogenation, usually referred to as CO_2 methanation, Power-to-Gas (PtG) (when H_2 is produced via water electrolysis with renewable electricity) or synthetic natural gas (SNG) production, is a highly exothermic reaction (Eq. 1) and the most thermodynamically favorable among the CO_2 hydrogenation reactions [7, 18, 20]. As a strongly exothermic process, CO_2 hydrogenation to CH_4 is favored at mild conditions, with CO_2 conversions up to 100% if carried below 200 °C [6]. On the other hand, at such temperature, the kinetics of the reaction is greatly affected. According to the proposed mechanisms, CO_2 hydrogenation to CH_4 can develop either by CO_2 reduction to CO with following CO methanation (Eq. 2), or by the formation of formate and carbonate intermediates on the catalyst surface [20, 21]. As both mechanisms involve an eight-electron transfer, the kinetics of this reaction is generally slow, especially if carried at low temperature [22, 23]. Higher temperatures (> 400 °C) may indeed favor the reaction kinetics, but thermodynamic limitations decrease CO_2 conversion to below 70% at 500 °C [20]. Moreover, the combination of higher process temperature with the exothermicity of this reaction may lead to increased CO production by competing reverse water–gas shift reaction (RWGS; Eq. 3) and to catalyst deactivation by sintering of the active metal particles and coke deposition by Boudouard reaction (Eq. 4) [7, 24].

$$\text{CO}_2\text{methanation:}\quad \text{CO}_2 + 4\text{H}_2 \rightleftharpoons \text{CH}_4 + 2\text{H}_2\text{O} \qquad \Delta H^{\circ}_{298\,\text{K}} = -165\,\text{kJ/mol} \tag{1}$$

$$\text{CO methanation:}\quad \text{CO} + 3\text{H}_2 \rightleftharpoons \text{CH}_4 + \text{H}_2\text{O} \qquad \Delta H^{\circ}_{298\,\text{K}} = -206\,\text{kJ/mol} \tag{2}$$

$$\text{Reverse water} - \text{gas shift(RWGS):}\quad \text{CO}_2 + \text{H}_2 \rightleftharpoons \text{CO} + \text{H}_2\text{O} \qquad \Delta H^{\circ}_{298\,\text{K}} = 41\,\text{kJ/mol} \tag{3}$$

$$\text{Boudouard reaction:}\quad 2\text{CO} \rightleftharpoons \text{C} + \text{CO}_2 \qquad \Delta H^{\circ}_{298\,\text{K}} = -172\,\text{kJ/mol} \tag{4}$$

Catalyst development for CO_2 hydrogenation to CH_4 is widely investigated in the literature due to the high interest in this process [24]. In this sense, novel alternative catalysts can pave the way towards more efficient process development and upscaling by overcoming the limitation of common and commercially available catalysts, especially related to the low activity at lower temperatures [6, 7]. Noble metals Ru and Rh, and transition metals Ni, Co, Fe and Mo are the

most commonly investigated active phases for CH_4 production via CO_2 hydrogenation, with especial attention to Ni-based catalysts, which are accepted as the most promising catalysts due to its satisfactory performance, abundance and low cost [25, 26], and to Co-based catalysts for its similar low cost and good catalytic activity for CO_2 conversion at low temperature [27]. However, the support phase also plays a major role on catalyst performance. Aspects such as metal-support interaction, active phase dispersion, catalyst stability, reducibility, oxygen mobility and electronic state of the metal active sites are directly influenced by the catalyst support [7, 28]. Furthermore, catalysts for CO_2 hydrogenation have a bi-functional activity, with the active metal particles being responsible for H_2 activation, while CO_2 activation occurs on the surface of the catalyst support [29, 30]. Metal oxides such as Al_2O_3, SiO_2, TiO_2, ZrO_2 and CeO_2 are the most commonly investigated catalyst supports and different studies have pointed out their contributing aspects for CO_2 hydrogenation, especially in terms of surface basicity (intrinsic or after modification) and metal dispersion [28, 31].

Hydroxyapatite (HAP, $Ca_{10}(PO_4)_6(OH)_2$) is a calcium phosphate-based material commonly used for medicine and water treatment applications [32] that has recently attracted increased attention as an alternative catalyst support. Previous reports have already pointed out the good performance of HAP-supported catalysts for processes such as dry reforming of methane (DRM, [33–40]), glycerol steam reforming [41] and photodegradation of water contaminants [42], for example. HAP presents several features that are required for a catalyst support. It presents high thermal stability, low water solubility, controllable surface acidity/basicity (in relation to the Ca/P ratio), oxygen mobility capacity and it can present a high surface area with both micro and mesopores structure depending on the synthesis method [36, 38, 43]. The basic aspect of stoichiometric HAP (Ca/P = 1.67) surface favors CO_2 adsorption and activation, as well as suppression of side reactions [44], while thermal stability and oxygen mobility may increase catalyst stability by avoiding sintering and coke accumulation [45, 46]. Such distinct features make HAP a potential catalyst support for CO_2 hydrogenation reactions.

Although numerous studies have already been dedicated to catalyst development for CO_2 hydrogenation, research effort is still required for improving catalyst performance [31]. Therefore, the present study aims to evaluate the performance of HAP as an efficient catalyst support for CO_2 hydrogenation for methane production as an alternative for classical and commercially available catalysts. Despite the already proven performance of HAP for other CO_2 conversion processes, such as DRM and photocatalytic processes [43, 47, 48], only one report, to the best of our knowledge, has considered HAP as a catalyst for methane production via CO_2 hydrogenation [44] with a clear focus on the presence of formate intermediates in the reaction mechanism, rather than on the process conditions. In this study, monometallic Ni, Co and Fe catalysts are chosen as active phases for their already reported utilization for CO_2 hydrogenation. Influences of temperature, metal load (Ni wt.%) and gas hourly space velocity (GHSV) are investigated for their effects on the performance of HAP-supported catalysts. Furthermore, for the first time in the literature, to the best of our knowledge, the performance of hydroxyapatite as catalyst support is demonstrated on semi-pilot scale, which is an important step to identify the potential and the challenges towards the scaling up of processes with alternative catalysts.

Materials and Methods

Catalyst Preparation

Commercial HAP (Ca/P = 1.67, 325 mesh, 60 m^2/g, Sigma-Aldrich, USA) was used as catalyst support without any further modifications. Nickel nitrate hexahydrate ($Ni(NO_3)_2.6H_2O$; > 98%, Alfa Aesar, USA), cobalt nitrate hexahydrate ($Co(NO_3)_2.6H_2O$; > 97.7%, Alfa Aesar, USA), iron nitrate nonahydrate ($Fe(NO_3)_3.9H_2O$; > 98%, Alfa Aesar, USA) and distilled water were used for catalyst preparation. All chemical products were used without any further modifications.

HAP-supported catalysts were prepared by incipient wetness impregnation (IWI) with 5–20 wt.% of active metals, as summarized in Table 1. For this synthesis, HAP support was impregnated with an aqueous solution containing the nitrate salts precursors of each metal. The aqueous precursor solutions were prepared at a desired concentration to deliver the appropriate amount of each metal to the support. After the impregnation step, the catalysts were dried overnight at 105 °C and calcined at 500 °C under static air atmosphere for 2 h.

Table 1 Summary of HAP-supported catalysts prepared in this work

Catalyst ID	Metal load (wt.%)		Particle size (nm)[b]
	Predicted	Measured[a]	
5Ni/HAP	5 wt.% Ni	4.2	17.5
10Ni/HAP	10 wt.% Ni	9.0	19.4
15Ni/HAP	15 wt.% Ni	14.0	16.8
20Ni/HAP	20 wt.% Ni	18.9	18.0
10Co/HAP	10 wt.% Co	9.4	16.4
10Fe/HAP	10 wt.% Fe	9.2	14.1

[a]As determined by Rietveld refinement

[b]As determined by Scherrer's equation

Catalyst Characterization

All characterizations were performed on powdered fresh catalysts previously calcined at 500 °C for 2 h. X-ray diffraction (XRD) spectra were obtained using a Phillips PANalytical X'Pert Pro MPD diffractometer with Cu Kα radiation (λ = 1.5406 Å) over a 2θ range of 20°–70° and a scan step size of 0.223°/s. The crystallite sizes of the impregnated particles (Ni, Co and Fe) were calculated using the Scherrer's equation. Metal content on the supported catalysts was determined by X-ray diffraction (XRD) using the Rietveld refinement. For that, all catalysts were calcined at 1000 °C for 5 h to ensure the formation of metal oxide crystalline phases and the spectra were acquired in the same conditions as described above. Scanning electron microscopy images with energy-dispersive X-ray spectroscopy (SEM–EDX) were obtained for evaluating the metal dispersion on the surface of the prepared catalysts. SEM–EDX images were acquired with a Hitachi microscope S-4700 coupled with a X-Max 50 detector (Oxford Instruments, UK) operating at 15.0 kV, under 1,000 times magnifications.

Catalyst Evaluation

CO_2 hydrogenation tests were carried in a semi-pilot scale fixed-bed stainless steel 316 reactor (id = 4.68 cm, h = 121.92 cm) under atmospheric pressure with a maximum flowrate of 10 L/min and can be operated with up to a few hundred grams of catalyst. Prior to each catalytic test, 10 g of each HAP-supported catalyst was diluted 1:10 with alumina sand (Al_2O_3–SiO_2, 30–40 mesh), placed in the center of the reactor supported by two quartz wool plugs, heated under N_2 atmosphere (500 mL/min) and reduced in situ with a mixture of 50 vol.% H_2/N_2 (500 mL/min) at 500 °C for 2 h. An electrical furnace with three heating zones was used for heating the reaction system, with a thermocouple placed in the center of the catalyst bed. After the reduction step, the system was cooled down to the test temperature under N_2 atmosphere (500 mL/min).

First, the influence of the temperature in the CO_2 hydrogenation was evaluated with the 10 wt.% metal-containing HAP supported catalysts (10Ni/HAP, 10Co/HAP and 10Fe/HAP). For evaluating the effect of temperature on the catalyst performance, CO_2 hydrogenation was carried at 250–500 °C at a gas hourly space velocity (GHSV) of 640 h^{-1}. At the working temperature, the reaction system was fed with a mixture of 4:1:0.5 of H_2:CO_2:N_2 at a total flow rate of 550 mL/min. Second, the influence of the metal load from 5 to 20 wt.% was assessed with the Ni-based catalysts (5Ni/HAP, 15Ni/HAP, 20Ni/HAP) at the same test conditions. Then, the influence of the GHSV was assessed at GHSV = 320–1600 h^{-1} at 350 °C for the best performing catalyst. Stability of the best performing catalyst was evaluated for 50 h of time-on-stream (TOS) at T = 350 °C and GHSV = 320 h^{-1}. Liquid products (H_2O) were separated from the outlet stream using a condensation system regulated at 4 °C and weighed. No further analysis was carried in the liquid portion. The volumetric flow rate and gas composition of the inlet gas were controlled by mass flow controllers (MFC; Brooks Instruments, USA). The volumetric flow rate of the dry outlet stream was measured with a digital flowmeter (model ADM1000; Agilent, USA). Quantification of reactants and reaction products was performed by gas chromatography (Bruker 456 GC) with three detectors TCD-TCD-FID. Conversions of CO_2 and H_2 (X_{CO_2} and X_{H_2}, respectively) and selectivity towards CH_4, CO and H_2O (S_{CH_4}, S_{CO} and S_{H_2O}, respectively) were calculated using Eqs. 5–9, where ṅ means the molar flow rate, *in* means inlet and *out* means outlet.

$$X_{CO_2}(\%) = \frac{\dot{n}_{(CO_2)in} - \dot{n}_{(CO_2)out}}{\dot{n}_{(CO_2)in}} * 100 \quad (5)$$

$$X_{H_2}(\%) = \frac{\dot{n}_{(H_2)in} - \dot{n}_{(H_2)out}}{\dot{n}_{(H_2)in}} * 100 \quad (6)$$

$$S_{CH_4}(\%) = \frac{\dot{n}_{(CH_4)out}}{\dot{n}_{(CO_2)in} - \dot{n}_{(CO_2)out}} * 100 \quad (7)$$

$$S_{CO}(\%) = \frac{\dot{n}_{(CO)out}}{\dot{n}_{(CO_2)in} - \dot{n}_{(CO_2)out}} * 100 \quad (8)$$

$$S_{H_2O}(\%) = \frac{\dot{n}_{(H_2O)out}}{\dot{n}_{(H_2)in} - \dot{n}_{(H_2)out}} * 100 \quad (9)$$

Results and Discussion

Catalyst Characterization

XRD spectra of the HAP-supported catalysts are presented on Fig. 1. The spectrum of the HAP supported was recorded without any further treatment and after calcination at 500 °C for 2 h under static air atmosphere (Fig. 1A). The characteristic diffraction peaks at 2θ = 25.9°, 31.8°, 32.9°, 34.1°, 39.8°, 46.7° and 53.2° match the hexagonal crystalline structure of hydroxyapatite (JCPDS 98-000-0251) in the planes corresponding to (002), (211), (300), (202), (222), and (004). Although no significant changes are observed in the spectrum after calcination, a decrease on the intensity of diffraction peaks observed at 2θ = 26.7° and 30.9° is consistent

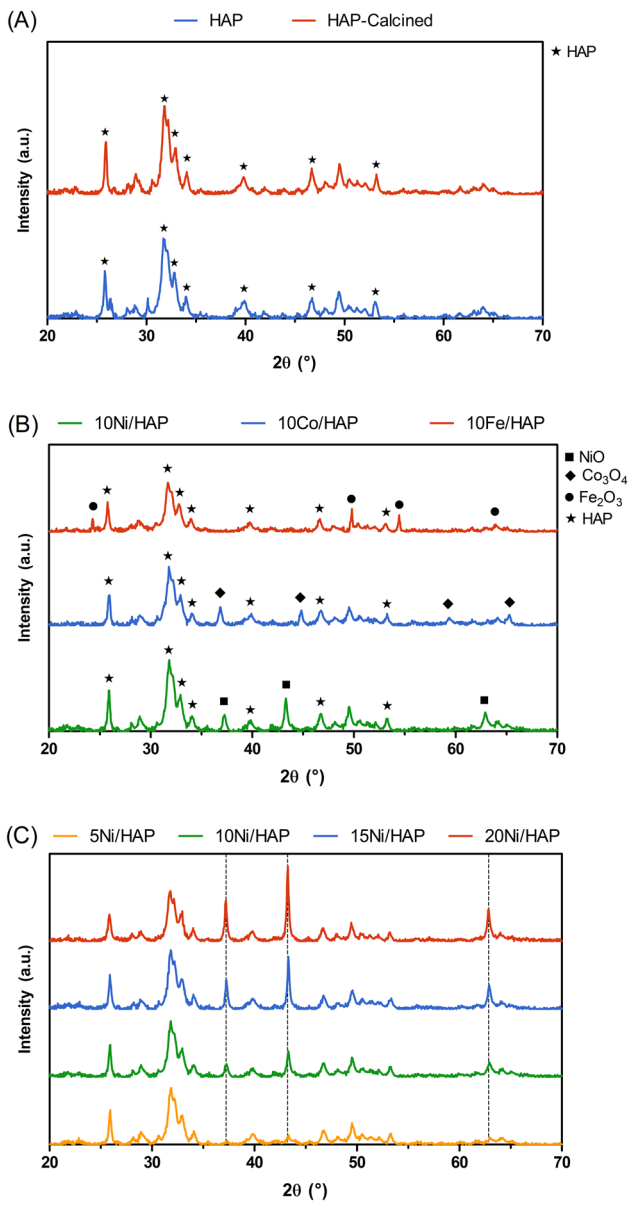

Fig. 1 XRD spectra for **A** non-treated and calcined HAP support, **B** 10 wt.% metal impregnated catalysts (10Ni/HAP, 10Co/HAP and 10Fe/HAP), and **C** Ni-impregnated catalysts (5Ni/HAP, 10Ni/HAP, 15Ni/HAP and 20Ni/HAP)

with the already reported increase in HAP crystallinity after calcination [49, 50].

For the 10 wt.% metal-impregnated catalysts, the XRD spectra can be seen on Fig. 1B. The formation of NiO, Co_3O_4 and Fe_2O_3 oxide phases is found on the impregnated catalysts. For 10Ni/HAP, diffraction peaks at 2θ = 37.3°, 43.3° and 62.9° (JCPDS 98-000-0133) correspond to a face-centered cubic crystalline phase and the (111), (200) and (220) planes for NiO. For 10Co/HAP, diffraction peaks at 2θ = 36.9°, 44.8°, 59.4° and 65.2° (JCPDS 98-000-0166) correspond to a face-centered cubic crystalline phase and the (311), (400), (511) and (440) planes of Co_3O_4. For 10Fe/HAP, diffraction peaks at 2θ = 24.2°, 49.8°, 54.4° and 64.1° (JCPDS 01-080-5406) correspond to a hexagonal crystalline phase and the (012), (024), (116) and (300) planes of Fe_2O_3. Figure 1C presents the XRD spectra for 5–20 wt.% Ni-based catalysts. Characteristic diffraction peaks at 2θ = 37.3°, 43.3° and 62.9° (marked by dashed lines) correspond to the (111), (200) and (220) planes of NiO (JCPDS 98-000-0133) and show a significant increase in intensity as the Ni load on the impregnated catalyst increase from 5 to 20 wt.%. In addition, no ion-exchanged hydroxyapatite structures are detected on the XRD, even for the Ni catalyst with higher loading (20 wt.%). This observation might be related to the conditions of the incipient wetness impregnation synthesis, where the lack of water excess does not favor ion exchange between the Ca^{2+} from the hydroxyapatite and the $Ni^{2+}/Co^{2+}/Fe^{3+}$ from the precursor solutions [34].

Catalyst metal load was assessed by the XRD spectra using the Rietveld refinement and results are presented on Table 1. The results show a good agreement between the calculated and measured amounts for all the HAP-supported catalysts. The impregnation yields ranged around 85–94%, which is expected for the synthesis via incipient wetness impregnation. Minor losses of metals during the synthesis process are usually related to the fixation of metals from the precursors solutions on the flask walls [34]. NiO, Co_3O_4 and Fe_2O_3 particle sizes were calculated from XRD spectra using the Scherrer's equation and are presented on Table 1. Results show that average particle sizes are in the range of 14–19 nm. For the Ni-impregnated catalysts, the increase on metal load from 5 to 20 wt.% did not represent a significant increase on particle size, which means that the increase on the metal load did not lead to agglomeration of the metal particles on the support's surface. As particle size did not significantly increase with the increase on metal load, a similar metal dispersion was maintained, which means that a higher portion of the catalyst surface was covered by metal particles/active sites.

To evaluate the distribution of metal particles on the surface of the HAP support, SEM–EDX was performed on the fresh calcined catalysts. Figure 2 presents the images at micrometric scale of the HAP support (Fig. 2A) and for the 10Ni/HAP (Fig. 2B), 10Co/HAP (Fig. 2C) and 10Fe/HAP (Fig. 2D) catalysts. EDX mapping shows the distribution of Ca and P from the structure of the HAP support and also highlights the good distribution of the impregnated metals (Ni, Co and Fe) on the surface of the support. In addition, Fig. 3 presents the SEM–EDX images acquired for all the Ni-based catalysts with increasing Ni load from 5 to 20 wt.%. Despite the increase on the metal load, the metal distribution on the surface of the support

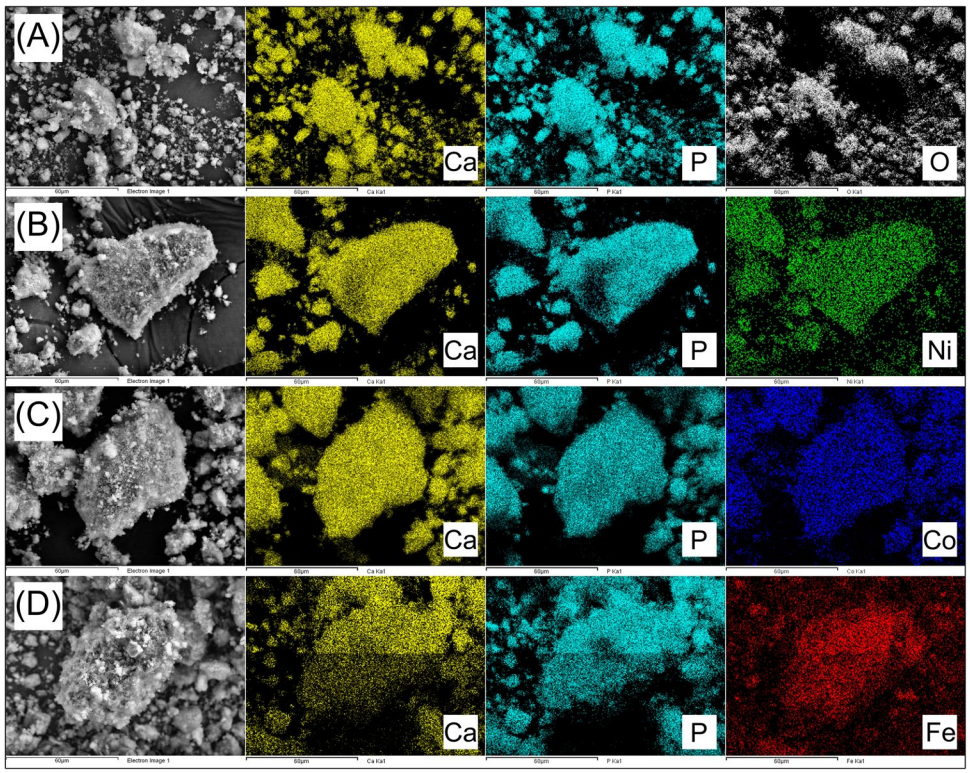

Fig. 2 SEM images of **A** HAP support, **B** 10Ni/HAP, **C** 10Co/HAP and **D** 10Fe/HAP at 1000 times magnification. EDX mapping showing the distribution of Ca (yellow), P (light blue), O (white), Ni (green), Co (blue) and Fe (red). Scale bar corresponding to 60 µm

did not seem to be affected by the higher Ni loadings, which confirms the hypothesis raised by the virtually unaltered average particle size, as calculated by the XRD spectra (Table 1).

Catalytic Performance of HAP-Supported Catalysts

In this study, the performance of HAP as an alternative support for classical catalysts for CH_4 production via CO_2 hydrogenation is evaluated with 10 wt.% Ni-, Co- and Fe-impregnated catalysts. The choice of the active phase is based on literature reports that already showed the use of Ni, Co and Fe for CO_2 hydrogenation processes, especially for CH_4 production [9, 10, 18, 51–53]. The performance of 10 wt.% HAP-supported catalysts is investigated at atmospheric pressure, GHSV = 640 h^{-1} on a semi-pilot scale fixed-bed reactor and over the temperature range from 250 to 500 °C. All fresh catalysts were submitted to in-situ reduction prior to the catalytic tests at 500 °C with a mixture with 50 vol.% H_2/N_2 at a total flowrate of 500 mL/min for 2 h. Previous studies on HAP-supported catalysts showed increased reducibility of active phases when compared to classical supports, such as Al_2O_3, for example, and reported that the reduction of the majority of metal particles should occur at temperatures below 500 °C, especially when the ion exchanged HAP structure were not present [34, 54, 55].

Catalytic performance of 10 wt.% HAP-supported catalysts is presented in Fig. 4. CO_2 and H_2 conversions (Fig. 4A, C, E) are presented along with the thermodynamic equilibrium data (black line) and product selectivity (Fig. 4B, D, F). The initial HAP support presents negligible activity towards CO_2 hydrogenation (data not shown). All catalysts present activity for CO_2 conversion between 250 and 500 °C. Initial CO_2 conversions at 250 °C are low around 10–16% for the three catalysts investigated. CO_2 conversions are favored by the temperature increase to a maximum of 70.4% for 10Ni/HAP at 400 °C (Fig. 4A), 62.3% for 10Co/HAP at 450 °C (Fig. 4C) and 61.0% for 10Fe/HAP at 500° (Fig. 4E). H_2 conversion follows similar trend at all conditions.

As an exothermic reaction favored at lower temperatures (Eq. 1), thermodynamics limits CO_2 conversion as temperature increases, despite the kinetics of CO_2 conversion not being favored at the low temperature range [22]. Maximum CO_2 conversion, according to the thermodynamic equilibrium, is around 98% at 250 °C but drops to around 90%, and then to below 70% as temperature increases to 350 °C and 500 °C, respectively [6]. For this reason, catalyst optimization towards maximizing CO_2 conversion at lower temperatures is necessary to overcome thermodynamic limitations. In this aspect, 10Co/HAP catalyst presents a slightly higher CO_2 conversion around 16.6% at 250 °C when compared to the other two evaluated catalysts (10Ni/HAP and 10Fe/HAP). On the other hand, the 10Ni/HAP achieves the highest CO_2 conversion (around 70.4%) at a lower temperature (T = 400 °C) when compared to the other

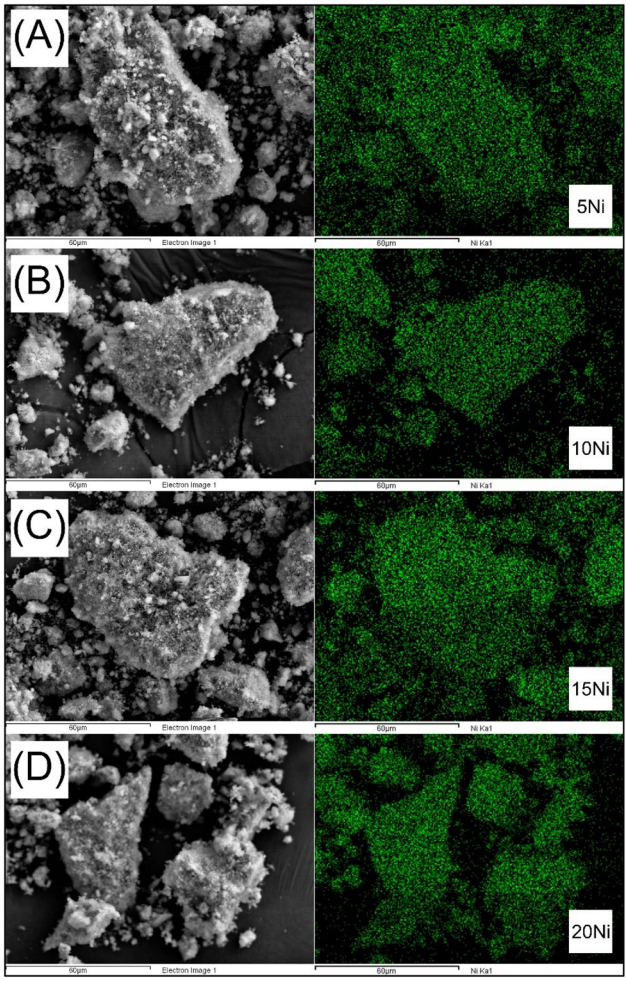

Fig. 3 SEM images of **A** 5Ni/HAP, **B** 10Ni/HAP, **C** 15Ni/HAP and **D** 20Ni/HAP at 1,000 times magnification. EDX mapping showing the distribution of Ni (green). Scale bar corresponding to 60 µm

two catalysts (450 °C and 500 °C for 10Co/HAP and 10Fe/HAP, respectively).

Product selectivity was calculated according to Eqs. 7–9. CH_4 and CO selectivity were expressed in relation to converted CO_2 (Eqs. 7 and 8, respectively) and H_2O selectivity was expressed in terms of converted H_2 (Eq. 9). No solid products (coke) were obtained during the reactions. Selectivity towards CH_4 is higher than 90% for the 10Ni/HAP and 10Co/HAP catalysts for temperatures up to 350 °C. For the 10Ni/HAP catalyst, CH_4 selectivity starts at 100% at 250 °C but it dropped to around 96.3% at 300 °C following a small production of CO, probably as a product of RWGS reaction (Eq. 3). CH_4 selectivity of 10Ni/HAP catalyst is stabilized above 90% up to 450 °C before dropping to 85.1% at 500 °C, when CO selectivity increases to 15%. As for 10Co/HAP, CH_4 selectivity also starts at 100% at 250 °C but drops to 93% at 350 °C, confirming the previously reported behavior of Co favoring CO_2 conversion and CH_4 selectivity at lower temperatures, when compared to Ni [53, 56]. However, as temperature increases, 10Co/HAP presents a higher activity to RWGS reaction. CO production also increases, with CO selectivity rising from around 9.0% to around 22%, from 400 to 500 °C. Literature showed that, although Co favors CH_4 production from CO_2 hydrogenation at lower temperatures, it also presents a higher activity towards RWGS reaction than Ni [57], which explains why the onset temperature for CO production is higher for 10Co/HAP when compared to 10Ni/HAP. However, as temperature increased, CO production was higher with 10Co/HAP.

As for 10Fe/HAP, product distribution is significantly different from the other two catalysts analyzed. CH_4 selectivity is low (below 15%) for the whole temperature range (250–500 °C), evidencing that RWGS was the dominant reaction. CO selectivity starts high at 100% and the onset temperature for CH_4 production is 350 °C, when CH_4 selectivity reaches 14.9%. As temperature increases, CH_4 selectivity slowly drops and reaches 10.4% at 500 °C. Literature showed that Fe presents significant activity towards RWGS reaction and favors the production of CO from a mixture of CO_2 and H_2, with major applications on syngas upgrading, for example [58, 59]. The behavior observed for 10Fe/HAP is consistent to the report by Kirchner et al. [52] that found a maximum yield of 8.0% towards CH_4, when investigating CO_2 hydrogenation over Fe-based catalysts. The authors also reported that increasing H_2/CO_2 ratio in the inlet feed leads to shifting the primary reaction towards CH_4 production, but for a maximum 59.0% CH_4 yield the required H_2/CO_2 ratio was 200. Furthermore, it is worth highlighting that, although the monometallic 10Fe/HAP catalyst does not present a significant activity for CH_4 production through CO_2 hydrogenation, several studies have evaluated the benefits of promoting Ni- and Co-based catalysts with Fe, for increasing their reducibility, sintering resistance and stability [53, 60, 61].

HAP-supported catalysts proposed in this work present a comparable performance for CO_2 hydrogenation when compared to similar catalysts reported in literature. Pieta et al. [18] reported the performance of Ni-based catalysts with different supports for CO_2 hydrogenation. Ni-based catalysts with Ni loads between 7 and 13 wt.% supported on Al_2O_3 and SiO_2 presented CO_2 conversion around 42% and 45%, respectively, at 350 °C. Comparatively, the 10Ni/HAP catalyst proposed in the present work present a CO_2 conversion around 60% at the same temperature (Fig. 4A). Liu et al. [62] evaluated the performance of mesoporous SiO_2 KIT-6-supported Co catalysts for CO_2 hydrogenation and reported a 40% CO_2 conversion at 340 °C, which was comparable to what was obtained with 10Co/HAP (36.7% CO_2 conversion at 350 °C, Fig. 4C). In a more recent study, Liu et al. [56] proposed a layered Co–Al–O catalyst for selective CO_2 hydrogenation at low temperature. For the catalysts prepared in a similar reduction temperature to

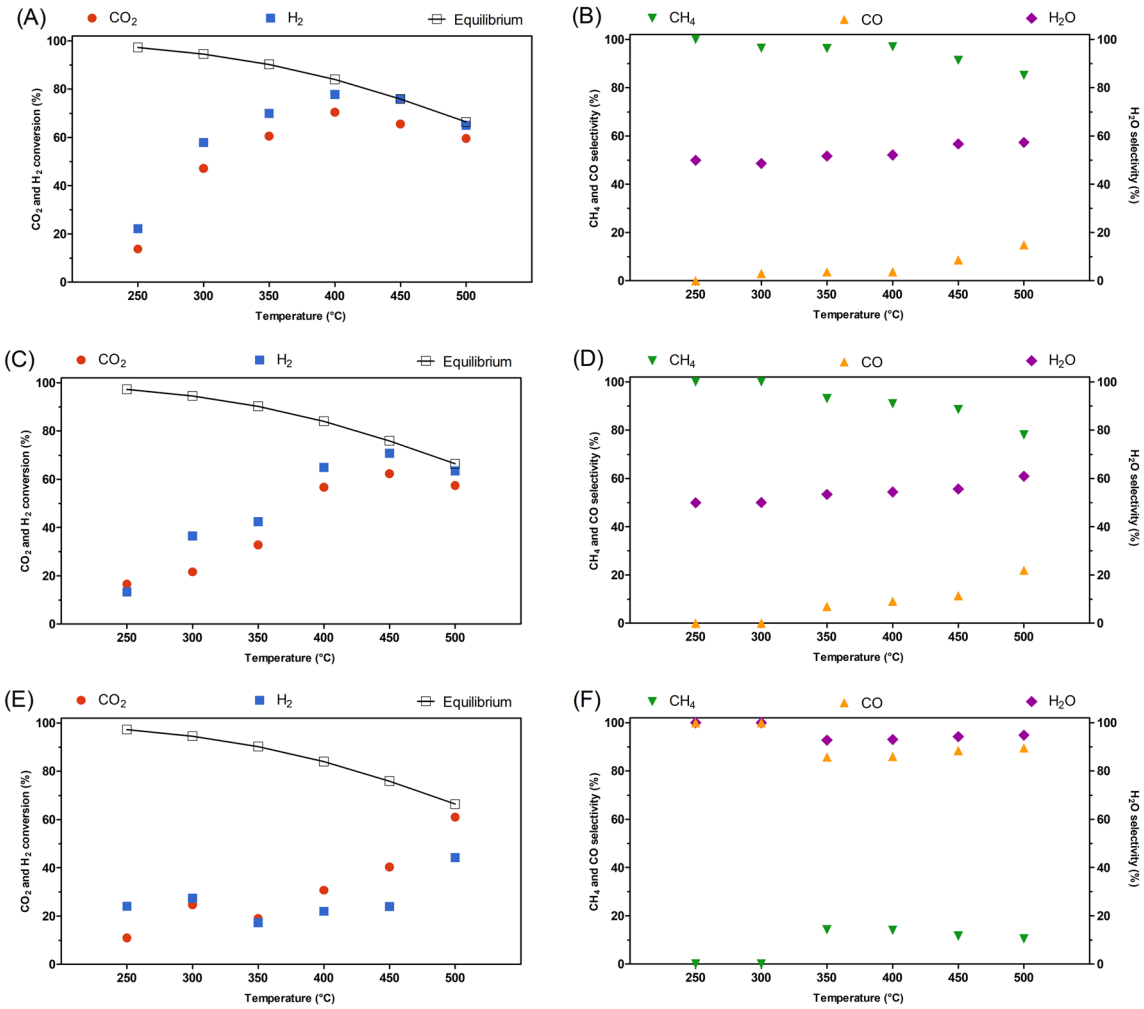

Fig. 4 Catalytic performance of **A**, **B** 10Ni/HAP, **C**, **D** 10Co/HAP and **E**, **F** 10Fe/HAP for CO_2 hydrogenation to CH_4 at T = 250–500 °C and GHSV = 640 h^{-1}. **A**, **C**, **E** CO_2 and H_2 conversions. **B**, **D**, **F** Selectivity towards CH_4 and CO, in relation to CO_2, and H_2O, in relation to H_2

the used in this work (500 °C), around 40% CO_2 conversion was achieved when CO_2 hydrogenation was carried at 250 °C and a maximum of 70% CO_2 conversion for catalysts prepared at higher reduction temperature (600 °C). These results show that further investigation on the structure of the active sites of Co-based HAP-supported catalysts can further improve its performance at lower temperatures. In terms of product selectivity, the decrease of CH_4 selectivity following an increasing CO production as temperature increases was unanimously reported by different studies [31, 51, 62, 63]. RWGS reaction is an endothermic reaction and literature reported the increasing competition between RGWS and CO_2 hydrogenation, with the favoring of RWGS, following a temperature increase [7, 64]. Finally, the HAP-supported catalysts proposed in this work presented a good performance for the CO_2 hydrogenation, especially in terms of favoring CO_2 conversion and CH_4 selectivity at lower temperatures (below 400 °C).

Despite the onset temperature for the start of CO production being lower for the 10Ni/HAP (CO production starting at 300 °C) than for 10Co/HAP (CO production starting at 350 °C), the maximum CO_2 conversion obtained with 10Ni/HAP is higher and it was achieved at a lower temperature (around 70.4% at 400 °C) when compared to 10Co/HAP (around 62.3% at 450 °C). For that reason, the Ni-based catalyst is chosen as the best performing HAP-supported catalyst for its potential for increasing CO_2 conversion and CH_4 selectivity at lower temperatures.

Influence of Ni Loading

The effects of Ni metal load as active phase for CO_2 hydrogenation to CH_4 over the HAP-supported catalysts is investigated in the range of 5–20 wt.%. Catalysts are similarly prepared by incipient wetness impregnation, calcined at 500 °C for 2 h at static air atmosphere and reduced with a

mixture of 50 vol.% H_2/N_2 at 500 °C for 2 h prior to testing. According to previous reports, the increase of metal loading on supported catalysts could lead, to a certain extent, to the increase on the number of active sites and facilitate electron transfer on the surface of the catalyst support, which could enhance the catalyst performance in terms of conversion and product selectivity [21, 65]. However, there whould be a limit for said improvement and, above a certain range, the increase on the catalyst load could lead to particle agglomeration, decrease on the active phase surface and favor catalyst deactivation [66]. Figure 5 presents the results of the performance of

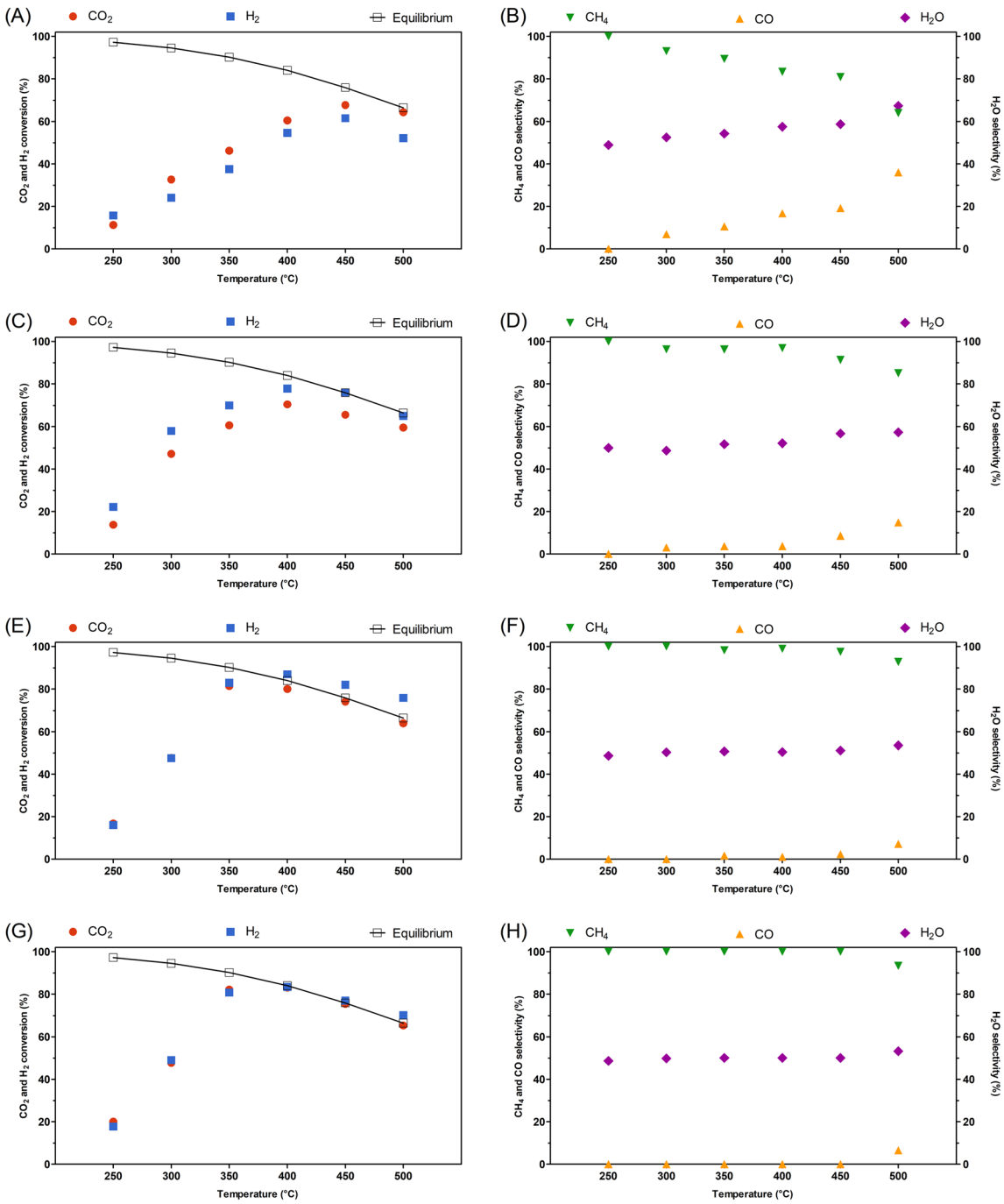

Fig. 5 Catalytic performance of **A**, **B** 5Ni/HAP, **C**, **D** 10Ni/HAP, **E**, **F** 15Ni/HAP and **G**, **H** 20Ni/HAP for CO_2 hydrogenation to CH_4 at T = 250–500 °C, GHSV = 640 h^{-1}. **A**, **C**, **E**, **G** CO_2 and H_2 conversions. **B**, **D**, **F**, **G** Selectivity towards CH_4 and CO, in relation to CO_2, and H_2O, in relation to H_2

HAP-supported catalysts prepared with 5–20 wt.% of Ni load at T = 250–500 °C and GHSV = 640 h^{-1}.

The increase on the Ni loading on the HAP-supported catalysts has a positive impact both on the conversion of CO_2 and on the selectivity towards CH_4. As observed in Fig. 5, the increase on the Ni loading both increases the maximum CO_2 conversion and shifts the peak of CO_2 conversion to lower temperatures. In addition, the higher Ni loadings also delays the onset temperature for the start of CO production, reducing the competition of RWGS reaction at lower temperatures. For 5Ni/HAP, CO_2 conversion starts at 11.2% at 250 °C and increases to a maximum of 67.6% at 450 °C (Fig. 5A). CO_2 conversion at 250 °C increases to 13.7%, 16.8% and 20.0% as Ni loading increases to 10 wt.%, 15 wt.% and 20 wt.%, respectively (Fig. 5C, E, G). Similarly, maximum CO_2 conversion increases to 70.4%, 80.0% and 83.1%, as Ni loading increases to 10 wt.%, 15 wt.% and 20 wt.%, respectively (Fig. 5C, E, G), and shifts from 450 °C (for the 5Ni/HAP) to 400 °C for the other three catalysts with higher Ni loadings (10–20 wt.%).

Furthermore, CO_2 conversion presents a linear increase with the temperature increase from 250 to 450 °C for 5Ni/HAP, with a slight decrease from 67.6% at 450 °C to 64.2% at 500 °C, following the decreasing thermodynamic limit of CO_2 conversion (Fig. 5A). For 15Ni/HAP (Fig. 5E) and 20Ni/HAP (Fig. 5G), CO_2 conversion presents a sharp increase between 250 and 350 °C, from 20 to 82.1%, respectively. From this temperature onwards, CO_2 conversion follows the decreasing behavior of the thermodynamic limit very closely, demonstrating the good performance of the Ni-based catalysts at higher Ni load (up to 20 wt.%).

Ni loading also influences the catalyst selectivity towards CH_4 production. CH_4 selectivity starts at 100% at 250 °C for all four catalysts evaluated. For 5Ni/HAP (Fig. 5B) and 10Ni/HAP (Fig. 5D), CH_4 selectivity drops at 300 °C to 93.0% and 96.3%, respectively. As temperature increases, maximum CO selectivity for 5Ni/HAP and 10Ni/HAP are 36.1% and 14.9% at 500 °C, respectively. In this case, although onset temperature for CO production is the same for both catalysts, the increase on Ni loading from 5 to 10 wt.% seems to reduce the occurrence of RWGS reaction both at 300 °C and 500 °C. For 15Ni/HAP (Fig. 5F), the onset temperature for CO production is 350 °C, higher than what was observed for 5Ni/HAP (300 °C) and 10Ni/HAP (300 °C), and CH_4 selectivity is higher than 90% at temperatures higher than 350 °C. For 20Ni/HAP catalyst, no CO production is detected up to 450 °C. At 500 °C, CH_4 selectivity is 93.4% for 20Ni/HAP, demonstrating that the increase on Ni loading up to 20 wt.% not only favors CO_2 hydrogenation at lower temperatures (300–350 °C), but it also decreases the occurrence of RWGS competing reaction even at higher temperatures (500 °C).

Similar behavior was previously described by Zhang et al. [64] and Cao et al. [67] for Ni-based catalysts supported on Al_2O_3 and mesoporous SiO_2 KIT-6, respectively. In both cases, the increase of Ni loading, up to a certain limit, was able to increase CO_2 conversion, CH_4 selectivity and delay the onset temperature for CO production by competing RWGS reaction. Zhang et al. [64] demonstrated that for 5 wt.% Ni load on Al_2O_3 support, RWGS is the primary reaction from 300 to 600 °C, with CH_4 yields below 10% while CO yields ranged from around 40% to around 50% at 450 °C and 600 °C, respectively. Although 5Ni/HAP catalyst prepared in this work did, in fact, favor the occurrence of RWGS reaction in the range of 300–500 °C (Fig. 5B), it is noteworthy that CO_2 hydrogenation to CH_4 was clearly the primary reaction while RWGS was rather a competing reaction gradually favored as temperature increased. Furthermore, Zhang et al. [64] also show that for Ni loadings between 12.5 and 50 wt.%, CO_2 hydrogenation to CH_4 is the main reaction at temperatures ranging from 300 to 500 °C, with a maximum CH_4 yield around 60% at temperatures ranging from 350 to 450 °C for catalysts containing 40–50 wt.% Ni.

Moreover, Cao et al. [67] reported that the increase in Ni loading from 10 to 40 wt.% on V-promoted mesoporous KIT-6-supported catalysts was able to shift the temperature of maximum CO_2 conversion from 425 °C (around 76.3% CO_2 conversion for 10Ni-0.5 V/KIT-6) to 350 °C (around 87.5% CO_2 conversion for 40Ni-0.5 V/KIT-6). CH_4 selectivity was also affected by the increase in Ni loading. However, authors demonstrated that the increase of the Ni loading was only beneficial up to 20 wt.%. At this range, CH_4 selectivity was kept at 100% up to 425 °C and onset temperature for CO production was at 450 °C. On the other hand, for the catalyst containing 40 wt.% Ni, CH_4 selectivity dropped to around 95% at 400 °C, as the further increase on the metal content led to the agglomeration of Ni particles and, in turn, to the favoring of RWGS reaction at lower temperature.

Based on the results presented here, the 20Ni/HAP was chosen as the best performing catalyst, due to its maximization of CO_2 conversion and CH_4 selectivity (delaying of the onset temperature of CO production). The evaluation of the influence of GHSV on the catalyst performance as well as the stability test for 50 h-long operation were performed with the 20Ni/HAP catalyst.

Influence of Gas Hourly Space Velocity (GHSV)

GHSV is an important parameter for evaluating catalytic performance, since it influences not only the fluid-dynamic of the system, but also the mass transfer on the catalyst surface [68]. The increase in the GHSV leads to a decrease in the residence time/contact time between the reactants (CO_2 and H_2) and the catalyst, and in the amount of species

adsorbed to the catalyst surface [23]. As both proposed mechanisms for CO_2 hydrogenation to methane (CO and formate intermediates) are relatively complex and include eight electron transfers [20, 21], the kinetics of the process tends to be very slow, especially at low temperatures. Moreover, low residence times present a negative impact on the catalyst performance, according to literature reports [69, 70]. From a process point of view, the GHSV is directly related to the sizing and flowrates of the catalytic systems, which, in turn, presents a direct impact on the costs of the process [71]. This is especially true at larger scale and it is a major challenge to be overcome during the upscaling process with alternative catalysts [72].

The influence of the GHSV over the HAP-supported catalysts performance was evaluated for the 20Ni/HAP catalyst at 350 °C. Although 350 °C was not the temperature for the maximum CO_2 conversion obtained with the 20Ni/HAP catalyst, at 400 °C the catalyst performance is already very close to the thermodynamic limit (Fig. 5G). For evaluating different GHSV conditions, the catalyst load on each test is kept the same and the total flow rate is adjusted according to the desired GHSV. Figure 6 presents the results for the catalytic performance of the 20Ni/HAP at GHSV varying between 320 and 1600 h^{-1}.

Both CO_2 and H_2 conversions are negatively affected by the increase in the process GHSV. An increase in CO_2 conversion, from 82.4% at 350 °C and 640 h^{-1} (Fig. 5G) to 87.9% at 350 °C and 320 h^{-1}, is achieved at the lowest GHSV tested (Fig. 6A). At GHSV = 320 h^{-1}, the maximum CO_2 conversion (87.9%) is relatively close to the thermodynamic limit expected for the CO_2 conversion during CO_2 hydrogenation (90.2% at 350 °C). A 5.0-fold increase in GHSV, from 320 to 1600 h^{-1}, results in a 12.5% decrease on CO_2 conversion, from 87.9 to 75.4%, respectively. H_2 conversion followed a similar behavior and drops from 86.9 to 76.4%, when the GHSV increases from 320 to 1600 h^{-1}. The positive influence of longer residence times (lower GHSV) has been reported in literature for CO_2 hydrogenation [26, 69, 70], as for other CO_2 conversion processes, such as dry reforming of methane [73] and biogas reforming [74], for example. Xiao et al. [26], when evaluating NiMgAl catalysts for CO_2 hydrogenation, reported that at GHSV = 15,000 h^{-1} not only maximum CO_2 conversion was higher (around 85%), but it was reached at lower temperature (T = 320 °C), than when compared with GHSV = 60,000 h^{-1} (around 70% CO_2 conversion at 360 °C). Similarly, Jaffar et al. [70] reported a decrease in CO_2 conversion from around 60% to around 30% following an increase on the GHSV from 3000 to 4800 mL h^{-1} g_{cat}^{-1}.

Selectivity towards CH_4 production is also affected by the change in the GHSV. CH_4 selectivity is at 100%, with no CO production, for GHSV ranging from 320 to 960 h^{-1} (Fig. 6B). At GHSV = 1280 h^{-1}, CH_4 selectivity drops to 95.1% and it continues dropping down to 92.2%, at GHSV = 1600 h^{-1}. On the other hand, CO production is observed for higher GHSV conditions (4.8% and 7.2% CO selectivity at 1280 h^{-1} and 1600 h^{-1}, respectively). H_2O selectivity is close to 50% at GHSV = 320–960 h^{-1} and it has a slight increase up to 53.1% at GHSV = 1600 h^{-1} as a result of a slight increase on H_2O production following CO production due to competing RWGS reaction. According to Stangeland et al. [23], as RWGS reaction is a more kinetically favorable reaction than CO_2 hydrogenation, higher GHSV are usually favorable to the competing CO production (via RWGS reaction) and detrimental to the CH_4 production (via CO_2 hydrogenation). Similar results have been reported by Xiao et al. [26] when evaluating the performance of Mn-promoted NiMgAl catalysts. The authors observed a slight decrease on CH_4 selectivity from 100% to around 95% following a 4.0-fold increase in GHSV, from 15,000 to 60,000 h^{-1}. Yeo et al. [75] have evaluated the influence of temperature, pressure and space velocity on the CO_2 methanation process using a 40Ni5Mg-Al-Zeolite catalyst by means of a Taguchi experimental design. In this study, the authors have reported that the reaction pressure had the highest influence on the catalyst performance, but the space velocity had

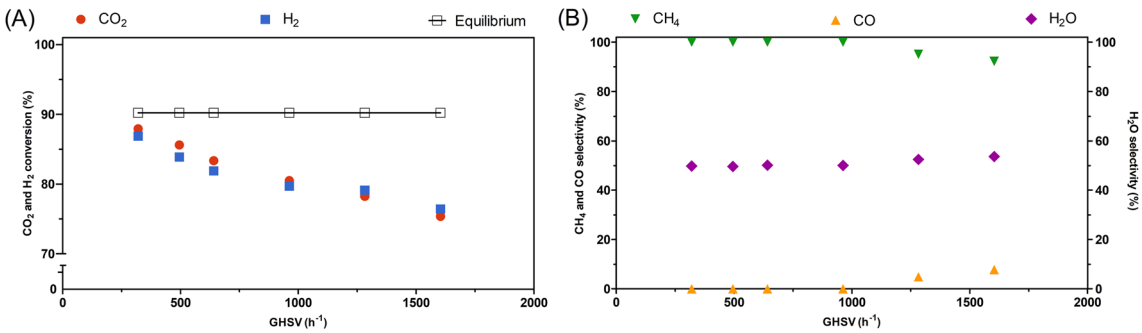

Fig. 6 Catalytic performance of 20Ni/HAP catalyst for CO_2 hydrogenation to CH_4 at T = 350 °C, GHSV = 320–1600 h^{-1}. **A** CO_2 and H_2 conversions. **B** Selectivity towards CH_4 and CO, in relation to CO_2, and H_2O, in relation to H_2

a greater influence than the reaction temperature. Furthermore, the authors reported achieving around 95% of CO_2 conversion and 90% of CH_4 yield at T = 315 °C, P = 19 bar and GHSV = 6,000 h^{-1}. Similar studies conducted by Jaffar et al. [70] and Han et al. [69] highlighted that the adsorption of both CO_2 and H_2 on the catalyst surface is significantly important for the success of CO_2 hydrogenation, mainly due to the complex reaction mechanism. The studies pointed out that the increase on GHSV can compromise the adsorption of reactants to the catalyst surface and further jeopardize the process performance, even when working far from thermodynamic limitations (e.g. low temperatures).

50 h-Long Stability Test

Best performing 20Ni/HAP catalyst was tested for 50 h-long catalytic stability in order to better assess the catalyst performance. The stability test was carried at 350 °C and GHSV = 320 h^{-1}, as the best optimized condition obtained from the tests with varied temperatures and residence times. Figure 7 presents the results for the long reaction test performed with this catalyst.

Figure 7 shows the robust performance of 20Ni/HAP for CO_2 hydrogenation to CH_4. 20Ni/HAP presents a high initial CO_2 conversion at 88.1% (Fig. 7A), which matches the good performance obtained in the previous test at GHSV = 320 h^{-1} (87.9% CO_2 conversion, Fig. 6A). CO_2 conversion slightly decreases to around 83% after 7 h of test and stabilizes around this value, with no signs of catalyst deactivation, for the whole duration of the test. The final CO_2 conversion obtained at TOS = 50 h was 82.8%. H_2 conversion follows a similar behavior and decreases from 89.4 to 84.3% by the end of the 50 h-long test. CH_4 selectivity is kept at 100% for the whole duration of the test (Fig. 7B). No signs of CO production and stable H_2O selectivity around 50% (Fig. 7B) demonstrate that the operation of the CO_2 hydrogenation reaction below thermodynamic limitations does not favor competing RWGS reaction.

Catalyst development is still one of the main challenges standing in the way of large-scale commercialization of CO_2 hydrogenation for CH_4 production [22]. In the process of developing new alternative catalysts, such as the HAP-supported catalysts proposed in this work, stability tests on larger scales (semi-pilot, pilot and demonstration, for example) are of great contribution for assessing the technology limitations and the associated risks for future steps [76], especially because information on large-scale testing and validation is so scarce. Few reports on literature show the feasibility of CO_2 hydrogenation for CH_4 (or SNG) production, including in the Power-to-Gas context, when CO_2 hydrogenation is carried out using captured CO_2 and clean H_2 coming from water electrolysis. Table 2 demonstrates the performance of the few large-scale (semi-pilot and pilot scales) reports on CO_2 hydrogenation. Data on the processes' performance is presented as reported in terms of CO_2 conversion and CH_4 production (CH_4 selectivity, CH_4 yield or CH_4 concentration on product stream). When compared to reported data on pilot scale, the performance of the 20Ni/HAP catalyst developed in this work, assessed at semi-pilot scale, is very promising in terms of CO_2 conversion, CH_4 selectivity and performance stability.

Conclusion

Hydroxyapatite has been proposed as an alternative catalyst support for CO_2 hydrogenation for CH_4 production. Ni-, Co- and Fe-based hydroxyapatite-supported catalysts have been prepared by incipient wetness impregnation and evaluated for CO_2 hydrogenation. The influences of temperature (250–500 °C), Ni metal load (5–20 wt.%) and GHSV (320–1600 h^{-1}) were investigated on semi-pilot scale conditions. CO_2 conversion was positively affected by the temperature increase, despite the thermodynamic limitations of the reaction. Although CO_2 hydrogenation is an exothermic reaction, no significant overheating was

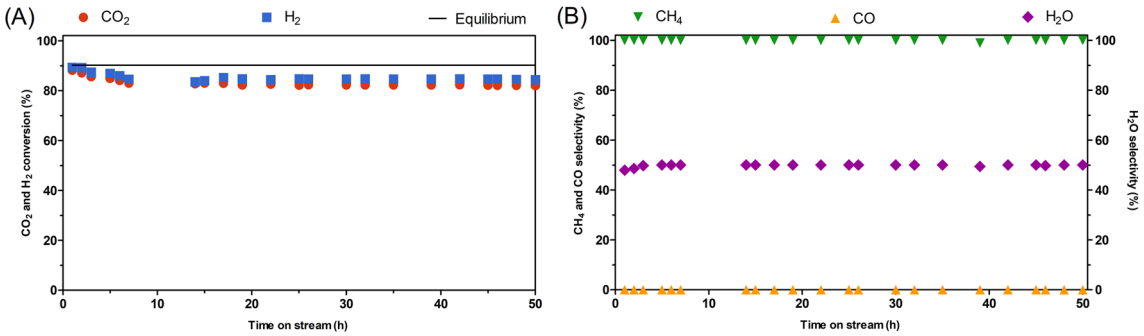

Fig. 7 Catalytic performance of 20Ni/HAP catalyst for CO_2 hydrogenation to CH_4 for 50 h of time on stream (TOS) at T = 350 °C, GHSV = 320 h^{-1}. **A** CO_2 and H_2 conversions. **B** Selectivity towards CH_4 and CO, in relation to CO_2, and H_2O, in relation to H_2

Table 2 Reports on large-scale CO_2 hydrogenation for CH_4 production

Process	Catalyst	Feed composition	Operation conditions	CO_2 conversion (%)	CH_4 production	TRL	References
Biogas hydrogenation	Ni-based	H_2:CO_2:N_2:He = 4.17:1:1.73:0.03, 1.4–2.3 $Nm^3.h^{-1}$	320 °C, 6.1 barg, bubbling fluidized-bed reactor, TOS = 1100 h	n.r	88% CH_4 yield	Pilot scale	[77]
Power-to-Gas	Ni-based	H_2:CO_2 = 4:1. 5.1–8.7 $kg.h^{-1}$	300 °C, 3 bar, microchannel tubular reactor, TOS = 100 h	Min. 93%	Min. 82 vol.% CH_4 on final SNG	Pilot scale	[78]
CO_2 hydrogenation	20 wt.% Ni-10 wt.% Ce/Zr	H_2:CO_2 = 4:1, GHSV = 1950 h^{-1}	300 °C, 1–1.2 bar,	86%	100% CH_4 selectivity	Pilot scale	[79]
CO_2 hydrogenation	25 wt.% Ni, 20 wt.% CeO_2, 55 wt.% Al_2O_3	H_2:CO_2 = 4:1, GHSV = 31,500 h^{-1}	320 °C, 5 bar, Two-staged microstructured tubular reactor, TOS = 2000 h	Min. 90%	Min. 92.5% CH_4 yield	Pilot scale	[80]
CO hydrogenation	Co-Fe-Al, (Co + Fe = 40 wt.%, Co/Fe = 1/3)	H_2:CO:N_2 = 72:24:4, 6,000 $mL.g^{-1}.h^{-1}$	300 °C, 10 bar, fixed-bed reactor, TOS = 24 h	60% CO conversion	59.3% CH_4 selectivity	Pilot scale	[61]
CO_2 hydrogenation	20Ni/HAP	H_2:CO_2:N_2 = 4:1:0.5, GHSV = 320 h^{-1}	350 °C, 1 bar, fixed-bed reactor, TOS = 50 h	Min. 83%	100%CH_4 selectivity	Semi-pilot scale	This work

TRL, Technology readiness level; SNG, Synthetic natural gas

detected on the system, even at high CO_2 conversion (max. 3–5 °C increase). For catalysts prepared with 10 wt.% of metal active phase (Ni, Co or Fe), CO_2 conversion ranged around 10–16% at 250 °C. Ni-based catalysts presented the best performance for CO_2 hydrogenation and maximum CO_2 conversion was around 70% at 400 °C and GHSV = 640 h^{-1} for 10Ni/HAP. Optimization of Ni metal load revealed that higher Ni content (up to 20 wt.%) had a positive impact on CO_2 conversion and delayed the onset of competing RWGS reaction. Further GHSV optimization revealed that longer residence times would benefit the slow CO_2 conversion, especially at lower temperatures. Best performing 20Ni/HAP catalyst was able to deliver a maximum CO_2 conversion around 88% at T = 350 °C and GHSV = 320 h^{-1}, with 100% CH_4 selectivity and no CO production up to 450 °C. Finally, long-term operation of 20Ni/HAP for 50 h on semi-pilot scale showed excellent catalytic performance with no significant signs of deactivation and a stable CO_2 conversion around 83% and 100% CH_4 selectivity. The results presented in this work demonstrate the feasibility of HAP as an alternative support for CH_4 production via CO_2 hydrogenation. Semi-pilot data shows the potential for process upscaling with alternative HAP-supported catalyst. Further studies should still focus on the possible modulation of HAP features for improving CO_2 conversion at even lower temperatures.

Funding The authors acknowledge financial support from the Materials for Clean Fuels (MCF) challenge program issued by the National Research Council Canada (NRC).

Data Availability Enquiries about data availability should be directed to the authors. Data will be made available upon request.

Declarations

Conflict of interest The authors declare no conflict of interest regarding the funding sources, or the materials used in the present study.

References

1. Bugaje, A.-A.B., Dioha, M.O., Abraham-Dukuma, M.C., Wakil, M.: Rethinking the position of natural gas in a low-carbon energy transition. Energy Res. Soc. Sci. **90**, 102604 (2022). https://doi.org/10.1016/j.erss.2022.102604
2. Jiang, W., Zhao, S., Yang, T.: Economic and technical analysis of power to gas factory taking Karamay as an example. Sustainability **14**, 5929 (2022). https://doi.org/10.3390/su14105929

3. European Commission: 2030 climate & energy framework, https://ec.europa.eu/clima/eu-action/climate-strategies-targets/2030-climate-energy-framework_en
4. Environment and Climate Change Canada: Canada's Climate Actions for a Healthy Environment and a Healthy Economy, Gatineau, QC (2021)
5. International Energy Agency: Total energy supply (TES) by source, World 1990–2019, https://www.iea.org/data-and-statistics/data-browser?country=WORLD&fuel=Energysupply&indicator=TESbySource
6. Liu, Z., Gao, X., Liu, B., Ma, Q., Zhao, T., Zhang, J.: Recent advances in thermal catalytic CO2 methanation on hydrotalcite-derived catalysts. Fuel **321**, 124115 (2022). https://doi.org/10.1016/j.fuel.2022.124115
7. Li, L., Zeng, W., Song, M., Wu, X., Li, G., Hu, C.: Research progress and reaction mechanism of CO_2 methanation over Ni-based catalysts at low temperature: a review. Catalysts **12**, 1–24 (2022). https://doi.org/10.3390/catal12020244
8. Zhang, Z., Liu, Y., Jia, L., Sun, C., Chen, B., Liu, R., Tan, Y., Tu, W.: Effects of the reducing gas atmosphere on performance of FeCeNa catalyst for the hydrogenation of CO_2 to olefins. Chem. Eng. J. **428**, 131388 (2022). https://doi.org/10.1016/j.cej.2021.131388
9. Witoon, T., Lapkeatseree, V., Numpilai, T., Kui Cheng, C., Limtrakul, J.: CO_2 hydrogenation to light olefins over mixed Fe–Co–K–Al oxides catalysts prepared via precipitation and reduction methods. Chem. Eng. J. **428**, 131389 (2022). https://doi.org/10.1016/j.cej.2021.131389
10. Witoon, T., Numpilai, T., Nijpanich, S., Chanlek, N., Kidkhunthod, P., Cheng, C.K., Ng, K.H., Vo, D.V.N., Ittisanronnachai, S., Wattanakit, C., Chareonpanich, M., Limtrakul, J.: Enhanced CO_2 hydrogenation to higher alcohols over K-Co promoted In_2O_3 catalysts. Chem. Eng. J. **431**, 133211 (2022). https://doi.org/10.1016/j.cej.2021.133211
11. Ren, M., Zhang, Y., Wang, X., Qiu, H.: Catalytic hydrogenation of CO_2 to methanol: a review. Catalysts **12**, 403 (2022). https://doi.org/10.3390/catal12040403
12. Ali, S.S., Ali, S.S., Tabassum, N.: A review on CO_2 hydrogenation to ethanol: reaction mechanism and experimental studies. J. Environ. Chem. Eng. **10**, 106962 (2022). https://doi.org/10.1016/j.jece.2021.106962
13. Visconti, C.G., Martinelli, M., Falbo, L., Infantes-Molina, A., Lietti, L., Forzatti, P., Iaquaniello, G., Palo, E., Picutti, B., Brignoli, F.: CO_2 hydrogenation to lower olefins on a high surface area K-promoted bulk Fe-catalyst. Appl. Catal. B Environ. **200**, 530–542 (2017). https://doi.org/10.1016/j.apcatb.2016.07.047
14. Bargiacchi, E., Antonelli, M., Desideri, U.: A comparative assessment of power-to-fuel production pathways. Energy **183**, 1253–1265 (2019). https://doi.org/10.1016/j.energy.2019.06.149
15. Sterner, M., Specht, M.: Power-to-gas and power-to-x—the history and results of developing a new storage concept. Energies **14**, 1–18 (2021). https://doi.org/10.3390/en14206594
16. Rego de Vasconcelos, B., Lavoie, J.-M.: Recent advances in power-to-X technology for the production of fuels and chemicals. Front. Chem. **7**, 1–24 (2019). https://doi.org/10.3389/fchem.2019.00392
17. CER: Canada's Energy Future 2019: Energy Supply and Demand Projections to 2040. (2019)
18. Pieta, I.S., Lewalska-Graczyk, A., Kowalik, P., Antoniak-Jurak, K., Krysa, M., Sroka-Bartnicka, A., Gajek, A., Lisowski, W., Mrdenovic, D., Pieta, P., Nowakowski, R., Lew, A., Serwicka, E.M.: CO_2 Hydrogenation to methane over Ni-catalysts: the effect of support and Vanadia promoting. Catalysts **11**, 433 (2021). https://doi.org/10.3390/catal11040433
19. Gorre, J., Ortloff, F., van Leeuwen, C.: Production costs for synthetic methane in 2030 and 2050 of an optimized power-to-gas plant with intermediate hydrogen storage. Appl. Energy **253**, 113594 (2019). https://doi.org/10.1016/j.apenergy.2019.113594
20. Gonçalves, L.P.L., Mielby, J., Soares, O.S.G.P., Sousa, J.P.S., Petrovykh, D.Y., Lebedev, O.I., Pereira, M.F.R., Kegnæs, S., Kolen'ko, Y.V.: In situ investigation of the CO2 methanation on carbon/ceria-supported Ni catalysts using modulation-excitation DRIFTS. Appl. Catal. B Environ. **312**, 121376 (2022). https://doi.org/10.1016/j.apcatb.2022.121376
21. Gao, X., Wang, Z., Huang, Q., Jiang, M., Askari, S., Dewangan, N., Kawi, S.: State-of-art modifications of heterogeneous catalysts for CO_2 methanation—active sites, surface basicity and oxygen defects. Catal. Today (2022). https://doi.org/10.1016/j.cattod.2022.03.017
22. Hussain, I., Jalil, A.A., Hassan, N.S., Hamid, M.Y.S.: Recent advances in catalytic systems for CO2 conversion to substitute natural gas (SNG): Perspective and challenges. J. Energy Chem. **62**, 377–407 (2021). https://doi.org/10.1016/j.jechem.2021.03.040
23. Stangeland, K., Kalai, D., Li, H., Yu, Z.: CO_2 methanation: the effect of catalysts and reaction conditions. Energy Procedia **105**, 2022–2027 (2017). https://doi.org/10.1016/j.egypro.2017.03.577
24. Lee, W.J., Li, C., Prajitno, H., Yoo, J., Patel, J., Yang, Y., Lim, S.: Recent trend in thermal catalytic low temperature CO_2 methanation: a critical review. Catal. Today **368**, 2–19 (2021). https://doi.org/10.1016/j.cattod.2020.02.017
25. Fan, W.K., Tahir, M.: Recent trends in developments of active metals and heterogenous materials for catalytic CO_2 hydrogenation to renewable methane: a review. J. Environ. Chem. Eng. **9**, 105460 (2021). https://doi.org/10.1016/j.jece.2021.105460
26. Xiao, X., Wang, J., Li, J., Dai, H., Jing, F., Liu, Y., Chu, W.: Enhanced low-temperature catalytic performance in CO_2 hydrogenation over Mn-promoted NiMgAl catalysts derived from quaternary hydrotalcite-like compounds. Int. J. Hydrog. Energy **46**, 33107–33119 (2021). https://doi.org/10.1016/j.ijhydene.2021.07.163
27. Summa, P., Świrk, K., Wang, Y., Samojeden, B., Rønning, M., Hu, C., Motak, M., Da Costa, P.: Effect of cobalt promotion on hydrotalcite-derived nickel catalyst for CO_2 methanation. Appl. Mater. Today **25**, 101211 (2021). https://doi.org/10.1016/j.apmt.2021.101211
28. Zhang, T., Wang, W., Gu, F., Xu, W., Zhang, J., Li, Z., Zhu, T., Xu, G., Zhong, Z., Su, F.: Enhancing the low-temperature CO_2 methanation over Ni/La-CeO_2 catalyst: the effects of surface oxygen vacancy and basic site on the catalytic performance. Appl. Catal. B Environ. **312**, 121385 (2022). https://doi.org/10.1016/j.apcatb.2022.121385
29. Hongmanorom, P., Ashok, J., Zhang, G., Bian, Z., Wai, M.H., Zeng, Y., Xi, S., Borgna, A., Kawi, S.: Enhanced performance and selectivity of CO_2 methanation over phyllosilicate structure derived Ni-Mg/SBA-15 catalysts. Appl. Catal. B Environ. **282**, 119564 (2021). https://doi.org/10.1016/j.apcatb.2020.119564
30. Garbarino, G., Wang, C., Cavattoni, T., Finocchio, E., Riani, P., Flytzani-Stephanopoulos, M., Busca, G.: A study of Ni/La-Al_2O_3 catalysts: a competitive system for CO_2 methanation. Appl. Catal. B Environ. **248**, 286–297 (2019). https://doi.org/10.1016/j.apcatb.2018.12.063
31. Aragüés-Aldea, P., Sanz-Martínez, A., Durán, P., Francés, E., Peña, J.A., Herguido, J.: Improving CO_2 methanation performance by distributed feeding in a Ni–Mn catalyst fixed bed reactor. Fuel (2022). https://doi.org/10.1016/j.fuel.2022.124075
32. Panda, S., Biswas, C.K., Paul, S.: A comprehensive review on the preparation and application of calcium hydroxyapatite: a special focus on atomic doping methods for bone tissue engineering. Ceram. Int. **47**, 28122–28144 (2021). https://doi.org/10.1016/j.ceramint.2021.07.100

33. De Vasconcelos, B.R., Lavoie, J.M.: Is dry reforming the solution to reduce natural gas carbon footprint? Int. J. Energy Prod. Manag. **3**, 44–56 (2018). https://doi.org/10.2495/EQ-V3-N1-44-56
34. Rego de Vasconcelos, B., Pham Minh, D., Martins, E., Germeau, A., Sharrock, P., Nzihou, A.: Highly-efficient hydroxyapatite-supported nickel catalysts for dry reforming of methane. Int. J. Hydrog. Energy **45**, 18502–18518 (2020). https://doi.org/10.1016/j.ijhydene.2019.08.068
35. Rego de Vasconcelos, B., Pham Minh, D., Martins, E., Germeau, A., Sharrock, P., Nzihou, A.: A comparative study of hydroxyapatite- and alumina-based catalysts in dry reforming of methane. Chem. Eng. Technol. **43**, 698–704 (2020). https://doi.org/10.1002/ceat.201900461
36. Phan, T.S., Sane, A.R., Rêgo de Vasconcelos, B., Nzihou, A., Sharrock, P., Grouset, D., Pham Minh, D.: Hydroxyapatite supported bimetallic cobalt and nickel catalysts for syngas production from dry reforming of methane. Appl. Catal. B Environ. **224**, 310–321 (2018). https://doi.org/10.1016/j.apcatb.2017.10.063
37. Tran, T.Q., Pham Minh, D., Phan, T.S., Pham, Q.N., Nguyen Xuan, H.: Dry reforming of methane over calcium-deficient hydroxyapatite supported cobalt and nickel catalysts. Chem. Eng. Sci. **228**, 115975 (2020). https://doi.org/10.1016/j.ces.2020.115975
38. Boukha, Z., Yeste, M.P., Cauqui, M.Á., González-Velasco, J.R.: Influence of Ca/P ratio on the catalytic performance of Ni/hydroxyapatite samples in dry reforming of methane. Appl. Catal. A Gen. **580**, 34–45 (2019). https://doi.org/10.1016/j.apcata.2019.04.034
39. Wang, Y.B., He, L., Zhou, B.C., Tang, F., Fan, J., Wang, D.Q., Lu, A.H., Li, W.C.: Hydroxyapatite nanorods rich in [Ca-O-P] sites stabilized Ni species for methane dry reforming. Ind. Eng. Chem. Res. **60**, 15064–15073 (2021). https://doi.org/10.1021/acs.iecr.1c02895
40. Meng, J., Pan, W., Gu, T., Bu, C., Zhang, J., Wang, X., Liu, C., Xie, H., Piao, G.: One-pot synthesis of a highly active and stable Ni-embedded hydroxyapatite catalyst for syngas production via dry reforming of methane. Energy Fuels **35**, 19568–19580 (2021). https://doi.org/10.1021/acs.energyfuels.1c02851
41. Dobosz, J., Cichy, M., Zawadzki, M., Borowiecki, T.: Glycerol steam reforming over calcium hydroxyapatite supported cobalt and cobalt-cerium catalysts. J. Energy Chem. **27**, 404–412 (2018). https://doi.org/10.1016/j.jechem.2017.12.004
42. Das, K.C., Dhar, S.S., Thakurata, D.G., Das, J.: Sn(II) inserted on hydroxyapatite encapsulated nickel ferrite (NiFe2O4@HAp-Sn2+): a novel nanocomposite for the effective photo-degradation of rhodamine B dye. J. Clean. Prod. **290**, 125172 (2021). https://doi.org/10.1016/j.jclepro.2020.125172
43. Bystrov, V.S., Piccirillo, C., Tobaldi, D.M., Castro, P.M.L., Coutinho, J., Kopyl, S., Pullar, R.C.: Oxygen vacancies, the optical band gap (Eg) and photocatalysis of hydroxyapatite: Comparing modelling with measured data. Appl. Catal. B Environ. **196**, 100–107 (2016). https://doi.org/10.1016/j.apcatb.2016.05.014
44. Wai, M.H., Ashok, J., Dewangan, N., Das, S., Xi, S., Borgna, A., Kawi, S.: Influence of surface formate species on methane selectivity for carbon dioxide methanation over nickel hydroxyapatite catalyst. ChemCatChem **12**, 6410–6419 (2020). https://doi.org/10.1002/cctc.202001300
45. Boukha, Z., de Rivas, B., González-Velasco, J.R., Gutiérrez-Ortiz, J.I., López-Fonseca, R.: Comparative study of the efficiency of different noble metals supported on hydroxyapatite in the catalytic lean methane oxidation under realistic conditions. Materials (Basel) **14**, 3612 (2021). https://doi.org/10.3390/ma14133612
46. Oh, S.C., Xu, J., Tran, D.T., Liu, B., Liu, D.: Effects of controlled crystalline surface of hydroxyapatite on methane oxidation reactions. ACS Catal. **8**, 4493–4507 (2018). https://doi.org/10.1021/acscatal.7b04011
47. Fatimah, I., Fahrani, D., Harmawantika, T., Sahroni, I., Kamari, A., Sa'bana Rahmatillah, C., Nurillahi, R.: Functionalization of hydroxyapatite derived from cockle (*Anadara granosa*) shells into hydroxyapatite–nano TiO_2 for photocatalytic degradation of methyl violet. Sustain. Environ. Res. **29**, 40 (2019). https://doi.org/10.1186/s42834-019-0034-3
48. Hu, M., Yao, Z., Liu, X., Ma, L., He, Z., Wang, X.: Enhancement mechanism of hydroxyapatite for photocatalytic degradation of gaseous formaldehyde over TiO_2/hydroxyapatite. J. Taiwan Inst. Chem. Eng. **85**, 91–97 (2018). https://doi.org/10.1016/j.jtice.2017.12.021
49. Panggabean, R.D., Yusuf, Y.: Preparation and characterization of hydroxyapatite based on human teeth with various of calcination. In: 2018 1st International Conference on Bioinformatics, Biotechnology, and Biomedical Engineering - Bioinformatics and Biomedical Engineering. pp. 1–4. IEEE (2018)
50. Hammood, A.S., Hassan, S.S., Alkhafagy, M.T., Jaber, H.L.: Effect of calcination temperature on characterization of natural hydroxyapatite prepared from carp fish bones. SN Appl. Sci. **1**, 436 (2019). https://doi.org/10.1007/s42452-019-0396-5
51. He, F., Zhuang, J., Lu, B., Liu, X., Zhang, J., Gu, F., Zhu, M., Xu, J., Zhong, Z., Xu, G., Su, F.: Ni-based catalysts derived from Ni–Zr–Al ternary hydrotalcites show outstanding catalytic properties for low-temperature CO_2 methanation. Appl. Catal. B Environ. **293**, 120218 (2021). https://doi.org/10.1016/j.apcatb.2021.120218
52. Kirchner, J., Anolleck, J.K., Lösch, H., Kureti, S.: Methanation of CO_2 on iron based catalysts. Appl. Catal. B Environ. **223**, 47–59 (2018). https://doi.org/10.1016/j.apcatb.2017.06.025
53. Sandupatla, A.S., Banerjee, A., Deo, G.: Optimizing CO_2 hydrogenation to methane over CoFe bimetallic catalyst: experimental and density functional theory studies. Appl. Surf. Sci. **485**, 441–449 (2019). https://doi.org/10.1016/j.apsusc.2019.04.217
54. Munirathinam, R., Pham Minh, D., Nzihou, A.: Hydroxyapatite as a new support material for cobalt-based catalysts in Fischer–Tropsch synthesis. Int. J. Hydrog. Energy. **45**, 18440–18451 (2020). https://doi.org/10.1016/j.ijhydene.2019.09.043
55. Campisi, S., Galloni, M.G., Marchetti, S.G., Auroux, A., Postole, G., Gervasini, A.: Functionalized iron hydroxyapatite as eco-friendly catalyst for NH 3 -SCR reaction: activity and role of iron speciation on the surface. ChemCatChem **12**, 1676–1690 (2020). https://doi.org/10.1002/cctc.201901813
56. Liu, Z., Gao, X., Liu, B., Song, W., Ma, Q., Zhao, T., Wang, X., Bae, J.W., Zhang, X., Zhang, J.: Highly stable and selective layered Co–Al–O catalysts for low-temperature CO_2 methanation. Appl. Catal. B Environ. **310**, 121303 (2022). https://doi.org/10.1016/j.apcatb.2022.121303
57. Sengupta, S., Jha, A., Shende, P., Maskara, R., Das, A.K.: Catalytic performance of Co and Ni doped Fe-based catalysts for the hydrogenation of CO_2 to CO via reverse water–gas shift reaction. J. Environ. Chem. Eng. **7**, 102911 (2019). https://doi.org/10.1016/j.jece.2019.102911
58. Castellanos-Beltran, I.J., Perreault, L.-S., Braidy, N.: Application of Ni–spinel in the chemical-looping conversion of CO_2 to CO via induction-generated oxygen vacancies. J. Phys. Chem. C. **125**, 7213–7226 (2021). https://doi.org/10.1021/acs.jpcc.1c00928
59. Putta, K.R., Pandey, U., Gavrilovic, L., Rout, K.R., Rytter, E., Blekkan, E.A., Hillestad, M.: Optimal renewable energy distribution between gasifier and electrolyzer for syngas generation in a power and biomass-to-liquid fuel process. Front. Energy Res. (2022). https://doi.org/10.3389/fenrg.2021.758149
60. Hwang, S., Hong, U.G., Lee, J., Baik, J.H., Koh, D.J., Lim, H., Song, I.K.: Methanation of carbon dioxide over mesoporous Nickel–M–Alumina (M = Fe, Zr, Ni, Y, and Mg) xerogel catalysts: effect of second metal. Catal. Letters. **142**, 860–868 (2012). https://doi.org/10.1007/s10562-012-0842-0

61. Kim, T.Y., Jo, S.B., Woo, J.H., Lee, J.H., Dhanusuraman, R., Lee, S.C., Kim, J.C.: Investigation of Co–Fe–Al catalysts for high-calorific synthetic natural gas production: pilot-scale synthesis of catalysts. Catalysts **11**, 105 (2021). https://doi.org/10.3390/catal11010105
62. Liu, H., Xu, S., Zhou, G., Huang, G., Huang, S., Xiong, K.: CO_2 hydrogenation to methane over Co/KIT-6 catalyst: effect of reduction temperature. Chem. Eng. J. **351**, 65–73 (2018). https://doi.org/10.1016/j.cej.2018.06.087
63. Zhou, G., Liu, H., Xing, Y., Xu, S., Xie, H., Xiong, K.: CO_2 hydrogenation to methane over mesoporous Co/SiO_2 catalysts: effect of structure. J. CO2 Util. **26**, 221–229 (2018). https://doi.org/10.1016/j.jcou.2018.04.023
64. Zhang, Z., Tian, Y., Zhang, L., Hu, S., Xiang, J., Wang, Y., Xu, L., Liu, Q., Zhang, S., Hu, X.: Impacts of nickel loading on properties, catalytic behaviors of Ni/γ–Al_2O_3 catalysts and the reaction intermediates formed in methanation of CO_2. Int. J. Hydrog. Energy. **44**, 9291–9306 (2019). https://doi.org/10.1016/j.ijhydene.2019.02.129
65. Shah, M., Das, S., Nayak, A.K., Mondal, P., Bordoloi, A.: Smart designing of metal-support interface for imperishable dry reforming catalyst. Appl. Catal. A Gen. **556**, 137–154 (2018). https://doi.org/10.1016/j.apcata.2018.01.007
66. Lv, C., Xu, L., Chen, M., Cui, Y., Wen, X., Li, Y., Wu, C., Yang, B., Miao, Z., Hu, X., Shou, Q.: Recent progresses in constructing the highly efficient Ni based catalysts with advanced low-temperature activity toward CO_2 methanation. Front. Chem. (2020). https://doi.org/10.3389/fchem.2020.00269
67. Cao, H., Wang, W., Cui, T., Wang, H., Zhu, G., Ren, X.: Enhancing CO_2 hydrogenation to methane by Ni-based catalyst with V species using 3D-mesoporous KIT-6 as support. Energies **13**, 2235 (2020). https://doi.org/10.3390/en13092235
68. Ascaso, S., Elena Gálvez, M., Da Costa, P., Moliner, R., Lázaro Elorri, M.J.: Influence of gas hourly space velocity on the activity of monolithic catalysts for the simultaneous removal of soot and NOx. Comptes Rendus Chim. **18**, 1007–1012 (2015). https://doi.org/10.1016/j.crci.2015.03.017
69. Han, D., Kim, Y., Byun, H., Cho, W., Baek, Y.: CO_2 Methanation of biogas over 20 wt% Ni-Mg–Al catalyst: on the effect of N_2, CH_4, and O_2 on CO_2 conversion rate. Catalysts **10**, 1201 (2020). https://doi.org/10.3390/catal10101201
70. Jaffar, M.M., Nahil, M.A., Williams, P.T.: Parametric study of CO_2 methanation for synthetic natural gas production. Energy Technol. **7**, 1–12 (2019). https://doi.org/10.1002/ente.201900795
71. Ha, S.-H., Kim, K.-H., Younis, S.A., Dou, X.: The interactive roles of space velocity and particle size in a microporous carbon bed system in controlling adsorptive removal of gaseous benzene under ambient conditions. Chem. Eng. J. **401**, 126010 (2020). https://doi.org/10.1016/j.cej.2020.126010
72. le Saché, E., Pastor-Pérez, L., Watson, D., Sepúlveda-Escribano, A., Reina, T.R.: Ni stabilised on inorganic complex structures: superior catalysts for chemical CO_2 recycling via dry reforming of methane. Appl. Catal. B Environ. **236**, 458–465 (2018). https://doi.org/10.1016/j.apcatb.2018.05.051
73. Chen, W.-H., Chiu, G.-L., Chyuan Ong, H., Shiung Lam, S., Lim, S., Sik Ok, Y., Kwon, E.: Optimization and analysis of syngas production from methane and CO_2 via Taguchi approach, response surface methodology (RSM) and analysis of variance (ANOVA). Fuel **296**, 120642 (2021). https://doi.org/10.1016/j.fuel.2021.120642
74. Xu, J., Zhou, W., Li, Z., Wang, J., Ma, J.: Biogas reforming for hydrogen production over a Ni–Co bimetallic catalyst: effect of operating conditions. Int. J. Hydrog. Energy. **35**, 13013–13020 (2010). https://doi.org/10.1016/j.ijhydene.2010.04.075
75. Yeo, C.E., Seo, M., Kim, D., Jeong, C., Shin, H.S., Kim, S.: Optimization of operating conditions for CO_2 methanation process using design of experiments. Energies (2021). https://doi.org/10.3390/en14248414
76. Rodney Turner, J.: The role of pilot studies in reducing risk on projects and programmes. Int. J. Proj. Manag. **23**, 1–6 (2005). https://doi.org/10.1016/j.ijproman.2004.01.003
77. Witte, J., Calbry-Muzyka, A., Wieseler, T., Hottinger, P., Biollaz, S.M.A., Schildhauer, T.J.: Demonstrating direct methanation of real biogas in a fluidised bed reactor. Appl. Energy. **240**, 359–371 (2019). https://doi.org/10.1016/j.apenergy.2019.01.230
78. Chwoła, T., Spietz, T., Więcław-Solny, L., Tatarczuk, A., Krótki, A., Dobras, S., Wilk, A., Tchórz, J., Stec, M., Zdeb, J.: Pilot plant initial results for the methanation process using CO2 from amine scrubbing at the Łaziska power plant in Poland. Fuel **263**, 116804 (2020). https://doi.org/10.1016/j.fuel.2019.116804
79. Ahn, J., Kim, H., Ro, Y., Kim, J., Chung, W., Chang, S.: Development of pilot-scale CO_2 methanation using pellet-type catalysts for CO_2 recycling in sewage treatment plants and its validation through computational fluid dynamics (CFD) modeling. Catalysts **11**, 1005 (2021). https://doi.org/10.3390/catal11081005
80. Guilera, J., Boeltken, T., Timm, F., Mallol, I., Alarcón, A., Andreu, T.: Pushing the limits of SNG process intensification: high GHSV operation at pilot scale. ACS Sustain. Chem. Eng. **8**, 8409–8418 (2020). https://doi.org/10.1021/acssuschemeng.0c02642

Authors and Affiliations

Fábio Gonçalves Macêdo de Medeiros[1] · Farbod Farzi[2] · Ines Esma Achouri[2] · Samira Lotfi[3] · Bruna Rego de Vasconcelos[1]

[1] Biomass Technology Laboratory, Department of Chemical and Biotechnological Engineering, Université de Sherbrooke, Sherbrooke, QC J1K 2R1, Canada

[2] Canada Research Chair (CRC) in Process Intensification for Advanced Catalysts and Sustainable Energy, Department of Chemical and Biotechnological Engineering, Université de Sherbrooke, Sherbrooke, QC J1K 2R1, Canada

[3] Energy, Mining and Environment Research Centre, National Research Council Canada, Ottawa, ON K1A 0R6, Canada